Subsurface deformations in nematic liquid crystals: The hexagonal lattice approach

G. Skačej,[1] V. M. Pergamenshchik,[2] A. L. Alexe-Ionescu,[3] G. Barbero,[4] and S. Žumer[1]
[1]*Physics Department, University of Ljubljana, Jadranska 19, 1000 Ljubljana, Slovenia*
[2]*Institute of Physics, Prospekt Nauky 46, Kiev-28, Ukraine*
[3]*Department of Physics, ''Politehnica'' University of Bucharest, Splaiul Independentei 313, 77206 Bucharest, Romania*
[4]*Dipartimento di Fisica del Politecnico di Torino, Corso Duca degli Abruzzi 24, 10129 Torino, Italy*
(Received 19 November 1996)

In this paper the existence of subsurface deformations in the orientational ordering of a nematic liquid crystal confined to a space between two planar substrates is studied by means of a lattice model. A superposition of the anisotropic induced-dipole–induced-dipole and isotropic Maier-Saupe interaction laws is used to describe intermolecular interactions in the nematic phase. To model the nematic phase we use a simple-hexagonal lattice, which does not introduce any bulk easy axes. The interaction nematic-confining surface (external anchoring) is described with the Rapini-Papoular form. We show that there is always a subsurface deformation in a layer of a few molecules when the intermolecular interaction law contains a nonzero fraction of the anisotropic interaction. The deformation is ascribed to the competition of external and effective intrinsic anchoring arising from the incomplete intermolecular interaction close to the surface. We also estimate the extrapolation length l_i as a measure of the intrinsic anchoring. This length turns out to be of molecular dimensions for the pronounced induced-dipole–induced-dipole character of the interaction. However, the corresponding subsurface deformation strength, given by the normal derivative of the director component, is considerably smaller than $1/l_i$, as the simplest estimate suggests. A realistic l_i can be achieved in our model only when the interaction anisotropy is considerably decreased. [S1063-651X(97)05507-4]

PACS number(s): 61.30.Cz, 61.30.Gd

I. INTRODUCTION

Nematic liquid crystals are anisotropic liquids consisting of rodlike molecules. The average orientation of the long molecular axis is described by the unit vector **n**, the director. In the absence of external forces and torques the molecules in an infinite sample or deep in the bulk tend to orient parallel to each other; then **n** is a constant vector $\mathbf{n}_0$. Any curvature of the director field $\mathbf{n}=\mathbf{n}(\mathbf{r})$ costs additional energy. The bulk elastic energy density is obtained by expanding the energy density in a power series of spatial director derivatives $n_{i,j}=\partial n_i/\partial r_j$ around the equilibrium state with $\mathbf{n}=\mathbf{n_0}$. At the lowest order in the derivative operator ∂ this expression has been derived by several authors (e.g., by Frank [1]) and can be written as

$$f_F(\mathbf{r})=\tfrac{1}{2}K_{11}[\boldsymbol{\nabla}\cdot\mathbf{n}]^2+\tfrac{1}{2}K_{22}[\mathbf{n}\cdot(\boldsymbol{\nabla}\times\mathbf{n})]^2+\tfrac{1}{2}K_{33}[\mathbf{n}\times(\boldsymbol{\nabla}\times\mathbf{n})]^2. \quad (1)$$

The three elastic constants correspond to three independent elastic modes: splay (K_{11}), twist (K_{22}), and bend (K_{33}). Expression (1) for the elastic energy density is valid only for an infinite sample. If the nematic sample has a bounding surface, there are two additional contributions to the lowest-order elastic energy density, which have been introduced long ago [2–4], but ignored for decades. The corresponding bulk elastic energy densities can be written as

$$f_{24}(\mathbf{r})=-K_{24}\boldsymbol{\nabla}\cdot[\mathbf{n}(\boldsymbol{\nabla}\cdot\mathbf{n})+\mathbf{n}\times(\boldsymbol{\nabla}\times\mathbf{n})], \quad (2)$$

$$f_{13}(\mathbf{r})=K_{13}\boldsymbol{\nabla}\cdot[\mathbf{n}(\boldsymbol{\nabla}\cdot\mathbf{n})], \quad (3)$$

where K_{24} (saddle-splay) and K_{13} (splay-bend) are the elastic constants connected with these contributions. Since these terms are total divergences, their bulk integrals can be converted by means of the Gauss theorem into surface integrals, so that they contribute only to boundary conditions. As such the constants K_{24} and K_{13} are also called surface-like. When **n** depends just on a single Cartesian coordinate, the K_{24} contribution vanishes identically. Furthermore, as discussed elsewhere, the K_{13} elastic term is renormalized by an elastic term linear in $n_{i,j}$ [5–7] and by the presence of surface fields [8]. For this reason, from now on k_{13} will indicate the effective splay-bend elastic constant, which takes into account these contributions.

Although they look similar, there is an important difference between the k_{13} and K_{24} contributions. The first one explicitly contains second-order derivatives in the components of **n**, whereas the second one does not. In terms of surface quantities this is shown to be equivalent to the presence of the normal-to-surface derivative in the surface density of the k_{13} term and its absence from that of the K_{24} term [9]. If one tries to find the director profile for, e.g., a nematic liquid crystal between two parallel plates using the standard variational procedure, these second-order derivatives produce mathematical difficulties, predicting a discontinuous director profile close to the surface of the sample [10,11]. On the other hand, the starting point of each continuum theory is an expansion based on weak deformations with respect to the molecular scale ρ_0 ($|n_{i,j}|\ll 1/\rho_0$). Now a paradox emerges [9], which is just due to cutting the infinite expansion at finite order (see also [12]). There are two approaches for dealing with the problem.

The first approach is the second-order elastic theory [13–15], which introduces one effective higher-order term into

the free-energy expansion in order to stabilize the distortion. The former discontinuity now disappears and changes into a very strong but continuous variation of the director over a distance of a few molecular dimensions. Its amplitude is proportional to the k_{13} elastic constant [7]. The predicted subsurface distortion is still too large to be consistent with the use of the continuum elastic theory ($|n_{i,j}| \sim 1/\rho_0$).

The other approach is the modified first-order theory [9]. The origin of this theory has been an *a priori* assumption that strong deformations are unphysical [9,16], and have to be suppressed by higher-order elastic terms. Surface effects such as subsurface deformations are disregarded in [9], and for a nematic liquid crystal between two parallel plates with symmetric anchoring this theory predicts a director profile with no subsurface deformation at all [17].

Recently, however, calculations in Refs. [5,6] showed that the total effect of the K_{13} term might be compensated by other surface elastic terms. In this case, a possible source of subsurface deformations can be anchoring. Indeed, in Ref. [9] it was shown that the bulk source of anchoring can be reduced to pure surface anchoring and a term formally identical to the K_{13} term.

The goal of this paper is to explore a nematic liquid crystal close to its surface using a simple molecular model that does not depend on any of the phenomenological approaches listed above. We would like to explore the possibility of deformations localized near the confining surfaces and try to determine their strength and mechanisms that drive them. Analyses of this kind, using a different interparticle interaction and the hypothesis of strong surface anchoring in a cubic lattice, continuum, or smecticlike approximation have been recently reported [18–20]. Our paper is aimed at studying a similar problem, but thoroughly reexamining the deformation strength, establishing a correlation between surface-induced deformations and forces acting in the nematic sample to find actual physical mechanisms thereof and the role of lattice-induced artifacts in orientational ordering described by lattice models.

We are going to deal with a nematic liquid crystal between two parallel plates, which is the simplest one-dimensional case. In Sec. II we propose a simple lattice model for the description of the nematic phase. The intermolecular pairwise interaction law is going to be composed of Maier-Saupe and induced-dipole–induced-dipole interactions, which can be responsible for the formation of the nematic phase [21]. We evaluate the total energy and find the director profile that minimizes it. The main results are presented and discussed in Sec. III.

II. MODEL

Let us consider a liquid crystal consisting of molecules, here described by molecular directors $\mathbf{n}$. For a pair of molecules with directors $\mathbf{n}=\mathbf{n}(\mathbf{R})$ and $\mathbf{n}'=\mathbf{n}(\mathbf{R}')$, separated by the vector $\mathbf{r}=\mathbf{R}'-\mathbf{R}$, we use a simple intermolecular pairwise interaction law

$$g_v(\mathbf{n},\mathbf{n}',\mathbf{r}) = -\frac{C}{r^6}\left[\mathbf{n}\cdot\mathbf{n}' - 3\frac{\varepsilon}{r^2}(\mathbf{n}\cdot\mathbf{r})(\mathbf{n}'\cdot\mathbf{r})\right]^2, \qquad (4)$$

where ε is the parameter of intermolecular interaction anisotropy, which varies between 0 and 1, while $C>0$ is the interaction strength constant. For $\varepsilon=0$ we obtain the Maier-Saupe interaction law, whereas for $\varepsilon=1$ the induced-dipole–induced-dipole law is obtained. The interaction law (4) has the same origin as the van der Waals interaction and includes (for $\varepsilon\neq 0$) anisotropic polarizability effects in nematic molecules. For $\varepsilon=0$ the interaction is spatially isotropic, i.e., not depending on the $\mathbf{r}$ direction. Then it just tends to orient nematic molecules parallel to each other everywhere in the sample, producing no subsurface deformation. Interesting cases are therefore those with $\varepsilon\neq 0$. Considering the interaction law (4), we take into account only long-range intermolecular interactions. It should be stressed that in our simple calculation short-range interactions, such as steric repulsions between molecules taken into account in continuous models [22] and in dynamic studies [23], will not be considered.

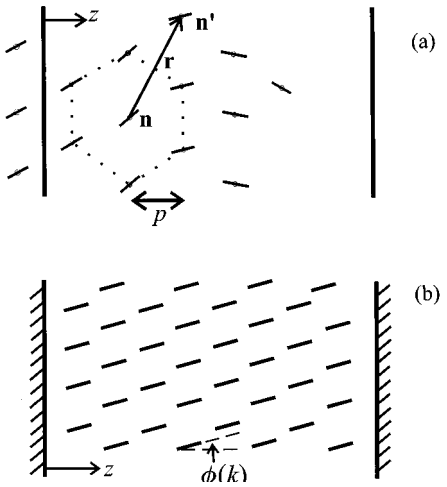

FIG. 1. (a) NLC sample between two parallel plates; the molecules are distributed into a hexagonal lattice. (b) The homogeneous sample; $\phi(k)$ is the molecular tilt angle in the kth layer.

A lattice version of the Maier-Saupe model ($\varepsilon=0$) for a nematic liquid crystal has been analyzed long ago using a Monte Carlo technique [24]. In Ref. [24] the authors showed that the nematic phase is stable in a given range of temperature. The nematic-isotropic phase transition is of first order, as experimentally observed. A similar analysis for $\varepsilon\neq 0$, to our knowledge, has not been done until now. A more sophisticated analysis based on the molecular-dynamics technique not using the lattice approximation has been published for a different kind of interparticle potential [25]. The results seem to indicate that the forces able to give rise to the nematic phase are the ones favoring side-to-side alignment. In Sec. III we will see that $\varepsilon\leqslant 0.3$ is required for the nematic state in our model. In this range of ε the interaction law (4) indeed favors side-to-side molecular alignment.

To simulate a liquid crystal, which is a continuous medium, on a lattice, one needs a model that does not introduce any artificial easy axes. Limiting our discussion to planar deformations, the molecules are allowed to rotate in parallel planes (xz planes) that are perpendicular to both walls (xy planes), while their mass centers are fixed to the lattice points. For our intermolecular interaction law the simple-hexagonal lattice with hexagons lying in xz planes, as shown in Fig. 1(a), introduces no bulk easy axis and thus satisfies

the above requirement. This kind of lattice is therefore more adequate for our purposes than the cubic lattice used in Ref. [18].

The lattice is characterized by spacing p between layers, where $p \to \rho_0$ ($\rho_0 \sim 1$ nm is the molecular dimension); see Fig. 1(a). We will consider a slab of N molecular layers. We parametrize the director by the tilt angle φ between the director and the surface normal z: $\mathbf{n}=(\sin\varphi,0,\cos\varphi)$, where $\varphi=\varphi(z)$. The dependence $\varphi=\varphi(z)$ has to be discretized according to the distribution of molecules in the sample. The same tilt angle $\phi(k)$ is thus assigned to all molecules in the kth molecular layer ($z=\text{const}$) for all $k \in [1,N]$, as shown in Fig. 1(b). Both bounding surfaces induce certain easy orientations ϕ_0, ϕ_1. This affects mostly those nematic molecules that lie close to the surface. In this analysis we are going to study only cases with symmetric external anchoring, where $\phi_0=\phi_1$. Further, we assume perfect nematic order, which means that the molecular director coincides with the nematic director $\mathbf{n}$ everywhere in the sample. This would be indeed true only for the perfectly ordered phase at zero temperature. Furthermore, we assume the particle density to be constant throughout the whole sample.

For the nematic-substrate interaction we assume [26]

$$g_s(\mathbf{n},\mathbf{\Pi},\mathbf{r}) = -\frac{C_1}{r^6}\,[\mathbf{n}\cdot\mathbf{\Pi}]^2, \tag{5}$$

where $\mathbf{\Pi}$ is the substrate-induced easy axis and $C_1>0$ a constant. Let us introduce the parameter $\eta_W = C_1/C$, which measures the relative strength of the nematic-substrate and nematic-nematic interactions. The anchoring at the nematic-substrate interface will be supposed comparable to the interaction responsible for the nematic phase. This means $\eta_W \sim 1$.

Now we must take into account all interactions between nematic molecules and their interactions with the substrate to obtain the total energy of the sample (F). Let us consider the bulk energy first. The position of each molecule is determined by a set of three numbers $\{\alpha,\beta,\gamma\}$, which are related to the spatial Cartesian coordinates x,y,z as follows: $x = p[2\alpha+\delta(\gamma)]/\sqrt{3}$, $y=p\beta$, and $z=p\gamma$. The function $\delta(\gamma)$ is equal to 1 if γ is even and 0 otherwise. In this way we can exploit the summation procedure already developed for the cubic lattice [18]. We denote the interaction energy of two molecules with positions $\{0,0,m\}$ and $\{\alpha,\beta,\gamma\}$ by $g_v(m;\alpha,\beta,\gamma)$. The total bulk energy of one molecule in the mth molecular layer can then be written as

$$f(m) = \sum_{\gamma=1}^{N}\sum_{\alpha=-\infty}^{\infty}\sum_{\beta=-\infty}^{\infty} g_v(m;\alpha,\beta,\gamma\neq m) + \sum_{\alpha=-\infty}^{\infty}\sum_{\beta=-\infty}^{\infty} g_v(m;\alpha\neq 0,\beta\neq 0,m), \tag{6}$$

where we must not count the contribution for $\alpha=\beta=0$ and $\gamma=m$ since this would represent the interaction of a molecule with itself. The intermolecular vector $\mathbf{r}$ can be written in terms of counters α,β,γ,m as $\mathbf{r}=p\{[2\alpha+\delta(\gamma)-\delta(m)]/\sqrt{3},\beta,\gamma-m\}$. The directors $\mathbf{n}$ and $\mathbf{n}'$ are expressed in terms of tilt angles $\phi(m)$ and $\phi(\gamma)$, according to the parametrization introduced above.

The total bulk energy of the sample per unit surface is obtained by summing single molecular energies (6) over layers (m)

$$F_v = \frac{\sigma}{2}\sum_{m=1}^{N}\left[\sum_{\gamma=1}^{N}\sum_{\alpha=-\infty}^{\infty}\sum_{\beta=-\infty}^{\infty} g_v(m;\alpha,\beta,\gamma\neq m) + \sum_{\alpha=-\infty}^{\infty}\sum_{\beta=-\infty}^{\infty} g_v(m;\alpha\neq 0,\beta\neq 0,m)\right], \tag{7}$$

taking only half of this sum not to count each interaction twice. Here $\sigma \propto 1/p^2$ stands for the molecular density per unit surface. In a similar way we calculate the interaction energy with the substrate for both plates. This is the external anchoring energy per unit surface:

$$F_s = \sigma\sum_{m=-M+1}^{0}\sum_{\gamma=1}^{N}\sum_{\alpha=-\infty}^{\infty}\sum_{\beta=-\infty}^{\infty} g_s(m;\alpha,\beta,\gamma,\phi_0) + \sigma\sum_{m=N+1}^{N+M}\sum_{\gamma=1}^{N}\sum_{\alpha=\infty}^{\infty}\sum_{\beta=-\infty}^{\infty} g_s(m;\alpha,\beta,\gamma,\phi_1), \tag{8}$$

where M is the number of layers by means of which the substrate is approximated. We are going to consider only cases with $\phi_0=\phi_1$.

If there is an external magnetic field, the corresponding energy F_B has to be taken into account as well. The energy of one molecule in the mth layer with the director $\mathbf{n}$ in the external magnetic field $\mathbf{B}$ can be written as $f_B(m) = -\int_{\mathbf{0}}^{\mathbf{B}}\mathbf{p}_B(m,\mathbf{B})\cdot d\mathbf{B}$, where $\mathbf{p}_B(m,\mathbf{B})$ stands for the field-induced magnetic moment of the molecule. The interaction energy of the nematic molecule with the external field then becomes [27] $f_B(m) = -\frac{1}{2}V_0\mu_0^{-1}\chi_\alpha[\mathbf{n}(m)\cdot\mathbf{B}]^2$, χ_a being the microscopic anisotropy of the molecular susceptibility, μ_0 the permeability of the vacuum, and V_0 the effective volume of one molecule. The total magnetic energy of the sample per unit surface in now given by

$$F_B = \sigma\sum_{m=1}^{N} f_B(m). \tag{9}$$

Here it is convenient to introduce another dimensionless parameter $\eta_B = V_0 p^6 \chi_\alpha B^2/2\mu_0 C$, which measures the strength of the magnetic interaction compared to the strength of the nematic-nematic one.

The total energy of the sample is composed of bulk and surface contributions plus the energy due to external fields, that is, $F=F_v+F_s+F_B$. We can hence induce deformations in the nematic sample through either external anchoring or external fields. Once all molecular orientations $\phi(k)$ are known, we can calculate the total energy F, which is then minimized with respect to all variables $\phi(k)$. This is accomplished by setting

$$\frac{\partial F}{\partial \phi(k)} = 0 \tag{10}$$

and $\partial^2 F/\partial\phi(k)^2 > 0$ for every $k \in [1,N]$ and then solving the system of nonlinear equations (10). This can be done for an

appropriate initial guess for the profile, e.g., with the multidimensional Newton ''tangential'' method. Here no ansatz for the director profile $\phi(k)$ is used, so we are not restricted to any particular class of functions. All calculations are very simple from the computer simulation point of view and can be carried out on ordinary personal computers within a reasonable amount of time.

III. RESULTS

Our intention is to simulate nematic liquid crystals. The director profiles in the bulk are therefore expected to be smooth. However, we are going to use the lattice approximation for this purpose, so we should expect that in certain cases solutions for director profiles correspond rather to the solid state than to soft matter such as nematic liquid crystals.

Each nematic molecule gives rise to an orienting field that strongly depends on the interaction anisotropy parameter ε. In a simplified picture, the neighboring molecules try to orient themselves as required by this field. For $\varepsilon=0$ the field consists of parallel lines only. No matter where the neighboring molecules are situated, they will orient parallel to the first molecule. In this way only a smooth nematic solution can be produced. For $\varepsilon\neq0$ the orienting field does not consist of parallel lines anymore. However, for low ε ($\varepsilon<0.4$) this field is still close to being parallel in the neighborhood of the molecule where the nearest neighbors are positioned. Therefore, the smooth nematic solution still represents the lowest-energy state. Further, in the high-ε range ($0.4<\varepsilon<1$) the orienting field close to the molecule becomes similar to the electric field of an electric dipole, directed along the long molecular axis. By decreasing ε this field is stretched along the long molecular axis, which results in the low-ε field form described above.

Let us now consider, in the high-ε regime, a molecule surrounded by the first six neighbors (in a plane), arranged into a hexagon, so that the long axis of the central molecule is, for example, parallel to two of the six sides of the hexagon. At the sites of the four neighbors belonging to these two sides, the dipolelike orienting field is far from being parallel with respect to the central molecule. However, due to symmetry reasons it is convenient for the four neighbors to take an orientation that is tilted 90° with respect to the central molecule. Such a configuration has significantly lower energy than the nematic one, in which all molecules are parallel to one another. In this way we can assemble an arbitrary sequence of tilts 0° and 90° throughout the nematic sample. This presents an example of a solid-state solution. However, also the smooth nematic solution still exists, but only for tilt angles close to either 0° or 90°, and it is metastable. For these reasons we should regard all solutions in the high-ε regime, including those of the nematic type, with care. In particular the briefly described solid-state solutions serve only as an illustration of lattice properties.

Let us now study the whole nematic sample. If there are, for example, no external fields, we can, for $\varepsilon>0.4$, indeed observe solutions with molecular tilt angles taking values of either 0° or 90°, changing from layer to layer in an arbitrary manner. The more switches between 0° and 90° a profile $\phi(k)$ contains, the lower its energy. The profile with the lowest energy is the one in which the tilt angle changes from 0° to 90° in each layer, i.e., the one containing the periodic angle sequence $\ldots$,0°, 90°, 0°, 90°, $\ldots$. In this family of solutions the profiles starting with 0°, 90°, 90°, 90°, $\ldots$ or 90°, 0°, 0°, 0°, $\ldots$ are also possible, which show an abrupt subsurface deformation of enormous strength. But as these profiles cannot be attributed to the nematic state, they must not be confused with subsurface deformations we intend to study. For this reason we shall from now on consider only $\varepsilon\leqslant0.3$, where the nematic phase seems to be stable. Such a restriction also ensures that side-to-side molecular alignment is favored, which is in agreement with the results of Ref. [25].

It should be stressed that in the cubic lattice model [18], for large ε, solid-state solutions have, in contrast to the hexagonal lattice, a considerably higher energy than nematic solutions, which is due to the different form of the lattice. This lattice, however, suffers from either the planar or homeotropic bulk easy axis.

In our model the liquid crystal has a limited size so that only finite numerical summations are performed. For practical reasons, i.e., saving computer time, we restrict the summation range even further (in samples with 71 layers to 17 molecular dimensions, while in those with 31 layers to 7 molecular dimensions), which can cause errors of a few percent when calculating director profiles, but does not change their qualitative character.

A. A slab of free nematic liquid crystal

Let us first consider a slab of nematic liquid crystal with no external anchoring or magnetic field. No external anchoring situation can be realized in practice on a nematic-vapor interface. In this manner we are able to explore effects due to incomplete intermolecular interactions. Molecular interaction volumes are not complete spheres for those molecules that lie close enough to the surface. If the intermolecular interaction is spatially anisotropic ($\varepsilon\neq0$), these incomplete interactions can cause certain orienting effects. Since in our model there is no orienting torque in the bulk, it suffices to consider the energy of the homogeneous sample only [$\phi(k)=\varphi_0=$const; see Fig. 1(b)].

If $\varepsilon=0$, all molecular orientations φ_0 give the same energy. This is no longer true for $\varepsilon\neq0$. For, e.g., $\varepsilon=0.3$, the solution with the lowest energy is the homeotropic homogeneous director profile ($\varphi_0=0°$). If nematic molecules are turned away from their preferred direction, the energy of the sample increases. This orienting effect is therefore a kind of anchoring. From now on we shall describe it by the term ''intrinsic anchoring'' since it is just due to the lack of intermolecular interactions. Its easy axis is homeotropic. This result is, to our knowledge, new for an intermolecular potential of the kind (4). The same result has been obtained in Ref. [23], where the Gay-Berne potential was used. To further explore the intrinsic anchoring, we calculate the energy F_0 of the homogeneous sample (per unit surface) for different φ_0. Dependences presented in Fig. 2 clearly show the observations listed above.

To characterize this intrinsic anchoring we introduce the intrinsic anchoring strength η_I (anchoring energy per unit surface) by fitting a parabola of the kind $\frac{1}{2}\eta_I\varphi_0^2$ to the F_0 vs φ_0 dependence (Fig. 2) close to the homeotropic easy axis of the intrinsic anchoring. The energy dependence for small de-

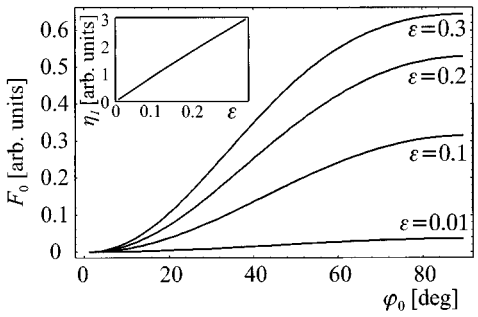

FIG. 2. Energy of the homogeneous sample F_0 vs tilt angle φ_0 for different ε. All curves have been shifted to the same starting point at $\varphi_0=0°$. In the inset the dependence intrinsic anchoring strength η_I vs ε is shown; the sample thickness is equal to $N=31$ layers.

viations from the easy axis is, like in the case of Rapini-Papoular anchoring, close to parabolic. The estimates for η_I are for various ε shown in the inset of Fig. 2. Instead of expressing η_I in terms of the interaction strength we express it through the de Gennes–Kléman extrapolation length $l_i = K/\eta_I$, where K stands for the Frank elastic constant (here $K_{11}=K_{22}=K_{33}=K$). Therefore, we must estimate the elastic constant K for our model. This can be achieved by comparing distortion energies calculated from the phenomenological approach and from the lattice model for a particular distorted profile. Since we would like to avoid effects of the k_{13} term, it is convenient to take an artificially bent profile, where the deformation is mainly concentrated in the bulk, e.g., $\varphi(z) = a/\{1+b(z-d/2)^2\}$, a and b being constants, and d the thickness of the sample [28]. For an appropriate choice of these parameters the k_{13}-term contribution to the distortion energy is negligible. The extrapolation length is now calculated by dividing the estimates for K and η_I. For $\varepsilon=0.3$ one finds $l_i \sim (1.6\pm0.2)\rho_0$; for $\varepsilon=0.2$, $l_i \sim (3.2\pm0.3)\rho_0$; for $\varepsilon=0.1$, $l_i \sim (8.0\pm1.0)\rho_0$; while for $\varepsilon=0.01$, $l_i \sim (100\pm10)\rho_0$, where $\rho_0 \sim 1$ nm is the molecular dimension (see Table I). The microscopic magnitude for the extrapolation length reported above for the most anisotropic interaction ($\varepsilon=0.3$) agrees with the one evaluated in the continuum approximation in Ref. [28]. A value of l_i in the molecular range has been reported in Ref. [22] as a consequence of the asymmetric shape of nematic molecules. Experimental results give, on the other hand, values over 100 nm for the extrapolation length [29]. This indicates that the intrinsic anchoring given by this calculation is of the same order as the experimentally determined anchoring only if ε is rather small ($\varepsilon \lesssim 0.01$). However, it is important to stress that it is very difficult to compare the extrapolation length estimated above with the one experimentally detected. In fact, as shown in Ref. [30], the value of l_i that is detectable results from all the interactions characterizing the nematic-substrate or nematic-vapor interface, for instance, steric, van der Waals, dipolar, and electrostatic interactions due to selective ions adsorption [31], which give rise to a kind of ''external'' contribution to the anchoring. In addition, in real systems close to the surface, we have also variations of elastic constants [32], scalar order parameters [33], density of mass, concentration of impurities [34], etc. These effects may change local elastic properties of the liquid crystal, resulting in a modification of the torque transmitted from the surface to the bulk and thus influencing the experimental determination of the anchoring energy.

TABLE I. Intrinsic anchoring extrapolation lengths l_i as estimated for the homogeneous sample and for the sample in the magnetic field, and the corresponding largest deformation amplitude $\Delta\phi$ in the latter case.

ε	$(l_i/\rho_0)_{\mathrm{hom}}$	$(l_i/\rho_0)_{\mathrm{mag}}$	$\Delta\phi_{\max}$ (deg)
0.01	100±10	110±10	0.75
0.1	8.0±1.0	8.5±1.0	6.9
0.2	3.2±0.3	3.2±0.3	14.9
0.3	1.6±0.2	1.6±0.2	24.1

B. A slab of free nematic liquid crystal in a magnetic field

In the preceding sub-section only undistorted director profiles were studied in order to extract information about intrinsic anchoring. Here we would like to repeat the estimation based on the simulation of distortions induced by a magnetic field in a free nematic slab. The magnetic field **B** determines the orientation of molecules in the bulk far from the surface while close to the surface it competes with the intrinsic anchoring if the angle α between the direction of **B** and the surface normal is not zero. The consequence is a deformation of the director profile. The amplitude of this deformation is denoted by $\Delta\phi=\phi_b-\phi_s$, where ϕ_b and ϕ_s stand for the bulk and surface tilt angles, respectively, the bulk tilt angle being measured in the middle of the sample. The molecules that are close to the surface gain more energy through intrinsic anchoring than they lose through changed magnetic and bend energies. The total energy is then lower than it would be if there was no distortion.

The phenomenological solution for the director profile $\varphi(z)$ can also be obtained from the ordinary Frank elastic theory by adding the $\frac{1}{2}\eta_I\varphi_0^2$ intrinsic anchoring form and the magnetic energy term [27] to Eq. (1) and then carrying out the ordinary variational minimization procedure. If the direction of the magnetic field α is close enough to the homeotropic intrinsic anchoring easy axis, we get a profile (for the symmetric sample) of the form

$$\varphi(z)=\alpha+A\,\frac{\cosh\left(\dfrac{z-d/2}{\xi}\right)}{\cosh\left(\dfrac{d}{2\xi}\right)}, \tag{11}$$

the parameter A being related to the amplitude of the deformation, d the sample thickness, and ξ the characteristic length of this field-induced deformation; the magnetic coherence length $\xi=\sqrt{K\mu_0/\chi_a B^2}$ [27]. In Fig. 3(a) director profiles for various values of the parameter $\eta_B \propto B^2$, i.e., for different field strengths, are shown. The stronger the magnetic field, the smaller the length ξ. The curves of the kind (11) (solid lines) with only one characteristic length (ξ) are in agreement with the profiles calculated from our model (dots). This means that all our profiles can be described by the Frank elastic theory, where the splay-bend contribution is

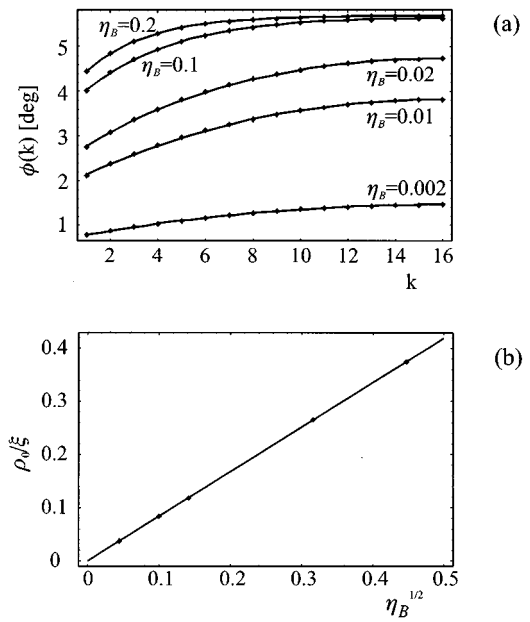

FIG. 3. Magnetic-field-induced distortions for $\varepsilon=0.1$ and different values of $\eta_B \propto B^2$; the angle between the field **B** and the surface normal is equal to $\alpha=0.1(180°/\pi)\approx 5.73°$. Dots denote calculated director profiles and solid lines the hyperbolic cosine fit. (a) The sample thickness is equal to $N=31$ layers. (b) The dependence ξ^{-1} vs $\eta_B^{1/2}$ for the upper case.

neglected. The main consequence of the interaction anisotropy ($\varepsilon\neq 0$) occurs in the form of intrinsic anchoring, which is here the source of the deformation. The characteristic length of this deformation varies with the magnetic-field strength. We are even able to check the proportionality $\xi \propto \eta_B^{-1/2} \propto B^{-1}$, from where it is possible to extract the value of the elastic constant K and to check the reliability of our fits [Fig. 3(b)]. This is an alternative method for the determination of K. However, it is not very precise since the effective molecular volume V_0 must be known.

If the magnetic field is strong enough, the bulk tilt angle can be determined by the direction of **B** ($\phi_b \sim \alpha$). For $\eta_B = 0.2$ the dependence $\Delta\phi \sim (\alpha - \phi_s)$ vs ϕ_s is shown in Fig. 4. We decide to put the actual surface tilt ϕ_s instead of the independent variable α along the abscissa, which enables us to compare this figure directly with Figs. 2 and 8, where the surface tilt angle is plotted along the horizontal axis too. For $\varepsilon \leqslant 0.3$ the sign of $\Delta\phi$ is positive and remains unchanged

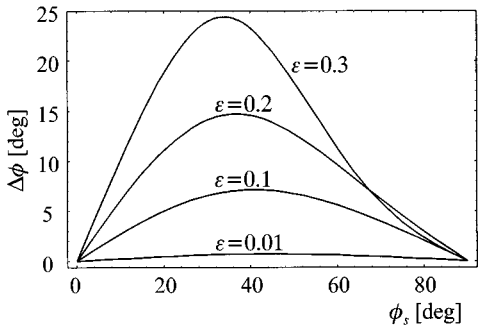

FIG. 4. Dependence $\Delta\phi$ vs ϕ_s for different ε. The bulk tilt is fixed by means of a magnetic field with $\eta_B=0.2$; $N=31$ layers.

through the whole range of ϕ_s. This is because for these ε the intrinsic anchoring easy axis is always homeotropic. The magnitude of $\Delta\phi$ is largest approximately where the corresponding curve in Fig. 2 has the highest slope. The amplitude $\Delta\phi$ increases with increasing ε, i.e., the intrinsic anchoring strength.

Since both parameters A and ξ can be obtained by fitting curves of the form (11) to the simulated curve, we can extract also the anchoring strength η_I. The intrinsic anchoring easy axis is denoted by ϕ_i. Routine calculations give the relation (for small $\phi_i - \alpha$)

$$l_i = \frac{K}{\eta_I} = \left[\frac{\phi_i - \alpha}{A} - 1\right] \xi \coth\left(\frac{d}{2\xi}\right), \tag{12}$$

from which we obtain the following estimates for the extrapolation length: for $\varepsilon=0.3$, $l_i \sim (1.6\pm 0.2)\rho_0$; for $\varepsilon=0.2$, $l_i \sim (3.2\pm 0.3)\rho_0$; for $\varepsilon=0.1$, $l_i \sim (8.5\pm 1.0)\rho_0$; and for $\varepsilon=0.01$, $l_i \sim (110\pm 10)\rho_0$, where $\rho_0 \sim 1$ nm again stands for the molecular dimension. These results agree with our estimates from Sec. III A, where the simplified case with the undistorted sample has been considered (see Table I).

The deformation of the director field is a result of the competition between intrinsic properties of the nematic and the external magnetic field. If the intermolecular potential is weakly anisotropic ($\varepsilon \ll 1$), the deformations are also weak, regarding director derivatives ($|n_{i,j}| \ll 1/\rho_0$). To become strong ($|n_{i,j}| \sim 1/\rho_0$), the action of two unrealistically strong couplings, the intrinsic anchoring, which is 10^2–10^3 times greater than actual nematic anchoring, and the magnetic field with the coherence length ξ of a few nanometers, is required [Figs. 3(a) and 4].

C. A slab of nematic liquid crystal with external anchoring

In previous sections we treated idealized cases without external anchoring and the deformation has been achieved through the action of the magnetic field competing with intrinsic anchoring. In real nematic cells there is always real surface anchoring, which in principle can have an easy axis, different from the one intrinsic anchoring favors. External anchoring, caused by the interaction between nematic molecules and the substrate, is, in contrast to magnetic field effects, strong only for those molecules that lie close to the surface. Since effects of the intrinsic anchoring are also restricted to a thin subsurface layer, it is now more difficult to predict the profile resulting from the competition of both anchorings. The external anchoring strength η_W can be also expressed in terms of the corresponding extrapolation length $l_e = K/\eta_W$, where K is determined as in Sec. III A. For instance, in case of $\eta_W=1$ and $\varepsilon=0.1$ this yields $l_e=(1.4\pm 0.2)\rho_0$, which is too short to describe the experimental values. Similarly to the case of intrinsic anchoring, a reasonable value of the extrapolation length can be obtained for a much weaker surface coupling ($\eta_W \lesssim 0.01$).

A deformation of amplitude $\Delta\phi$ now appears in a thin subsurface region of only 2–3 molecular layers (see Figs. 5 and 6). Its magnitude depends on ε (which regulates the intrinsic anchoring strength), the external anchoring strength η_W, and the corresponding easy direction ϕ_0. In the bulk the tilt angle approaches the constant value ϕ_b, as predicted

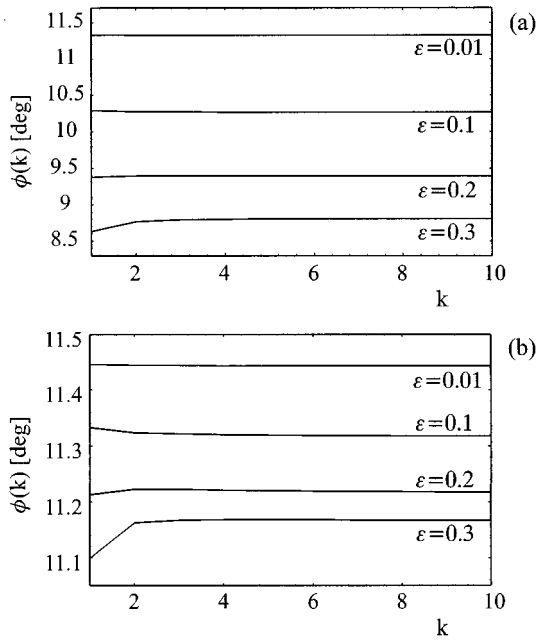

FIG. 5. Director profiles in a sample with noncontact external anchoring for different ε. The easy axis $\phi_0=0.2(180°/\pi)\approx 11.46°$, the anchoring strength (a) $\eta_W=1$ and (b) $\eta_W=10$, and $N=71$ layers.

from the Frank theory. Each profile is characterized by two main features: the surface tilt ϕ_s and the amplitude of the deformation $\Delta\phi=\phi_b-\phi_s$.

In order to understand the source of the deformation we shall have a closer look at the effects of intrinsic anchoring. The largest contribution to the intrinsic anchoring comes from molecules that are closest to the surface, i.e., lying in the first subsurface layer of the liquid-crystal sample. Since

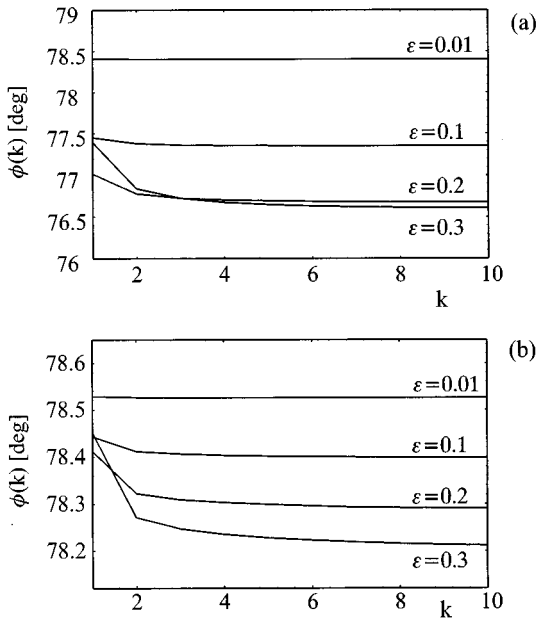

FIG. 6. Director profiles in a sample with noncontact external anchoring for different ε. The easy axis $\phi_0=(\pi/2-0.2)(180°/\pi)\approx 78.54°$, the anchoring strength (a) $\eta_W=1$ and (b) $\eta_W=10$, and $N=71$ layers.

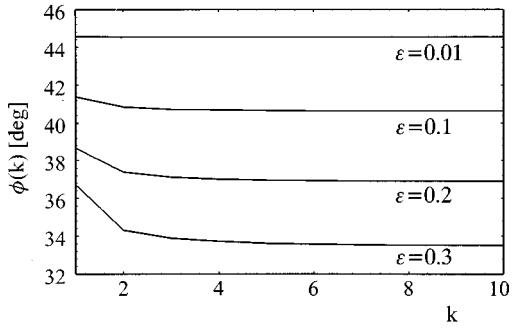

FIG. 7. Director profiles in a sample with contact external anchoring for various ε. The external anchoring easy axis $\phi_0=45°$, the anchoring strength $\eta_W=1$, and $N=31$ layers.

the intermolecular interaction does not abruptly vanish over one molecular dimension, molecules deeper in the bulk also contribute to the intrinsic anchoring, but to a much smaller extent. For these molecules the intrinsic anchoring-induced easy axes can, due to different geometry, differ from those induced by the first layer alone. For our interaction, which decreases relatively fast with increasing distance, the major contribution to the intrinsic anchoring energy of the whole sample arises from the first molecular layer and the contributions of the following ones are small enough that they do not influence the easy axes anymore.

The surface tilt ϕ_s is determined by the competition of external and intrinsic anchoring in the first molecular layer, favoring ϕ_0 and ϕ_i, respectively. The angle ϕ_s always takes a value between ϕ_0 and ϕ_i. In the deeper-lying layers the effects of both kinds of anchoring are considerably weaker, but still of comparable strength in contrast to the magnetic case (Sec. III B), where the magnetic-field strength remained unchanged throughout the sample. In order to explain the sign of $\Delta\phi$, we must again compare effects of both anchorings, now studying layers that follow the first one. The intrinsic anchoring strength can, depending on ε and ϕ_s, decrease slower or faster in comparison to external anchoring when penetrating into the bulk. Then effects of the slower-decreasing anchoring are the ones that prevail there. Moreover, intrinsic anchoring-induced easy axes are also ε dependent and, as already stated, not necessarily the same as in the first layer.

These phenomena are much more evident if we use a contact potential for external anchoring acting only in the first molecular layer, but having otherwise the same form as in Eq. (5). Such an anchoring could be due, e.g., to steric surface effects. In this case the molecular tilt in a certain layer beyond the first one is determined by intrinsic anchoring only. Some director profiles for this kind of anchoring are presented in Fig. 7. For $\varepsilon\leqslant 0.3$, $\Delta\phi$ is negative, according to intrinsic anchoring, which in this range of ε favors $\phi_i=0°$ also for the layers beyond the first one (the external contact anchoring easy axis is here $\phi_0=45°$).

In the rest of our discussion only noncontact external anchoring will be treated. The dependence $\Delta\phi$ vs ϕ_s for such an anchoring is shown in Fig. 8 and is significantly different from the one obtained for the magnetic-field-induced deformation (Fig. 4). There are two regimes regarding the behavior of $\Delta\phi$ if we change ϕ_s (Fig. 8) (a) For $\varepsilon\leqslant 0.1$ the sign of

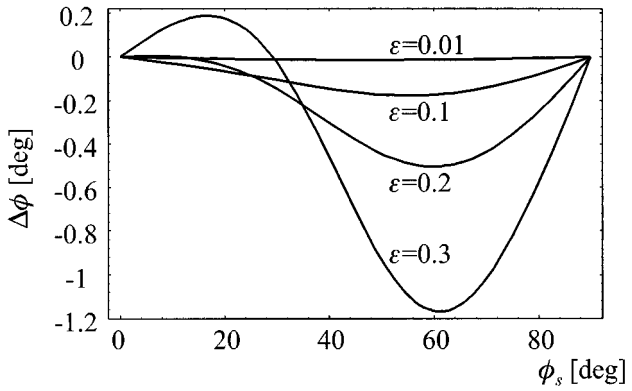

FIG. 8. Dependence $\Delta\phi$ vs ϕ_s in a sample with noncontact external anchoring ($\eta_W=1$) for different ε; $N=31$ layers.

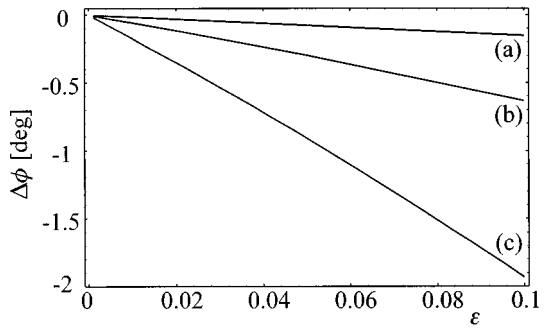

FIG. 9. Dependence $\Delta\phi$ vs ε in a sample with external anchoring, with $\eta_W=1$, $\phi_0=45°$, and $N=31$ layers: (a) noncontact anchoring, (b) contact anchoring, and (c) the theoretical prediction with the bare K_{13} constant.

$\Delta\phi$ remains unchanged through the whole range of ϕ_s and is, in contrast to the magnetic-field case, negative. In this case intrinsic anchoring effects, favoring $\phi_i=0°$ in all layers, decrease slower than external anchoring effects, favoring $\phi_0 \neq \phi_i$, when penetrating into the bulk. Therefore, in the bulk intrinsic anchoring prevails and moves the tilt towards $\phi_i=0°$. (b) For $0.1<\varepsilon\leqslant 0.3$ all this is true only for large ϕ_s, which again gives a negative $\Delta\phi$, while for the small ones it is just the opposite: external anchoring effects decrease slower than the intrinsic ones; $\Delta\phi$ is then positive. The intrinsic anchoring-induced easy axis is here the same as for $\varepsilon\leqslant 0.1$, that is, homeotropic.

Another parameter that can be varied is the external anchoring strength η_W. In Figs. 5 and 6 we show the director profiles only for very strong anchoring ($\eta_W=1,10$), where differences in the behavior for different ε are clearly visible. If η_W is large, i.e., $l_e \ll l_i$, $\Delta\phi$ becomes small since the substrate-induced orienting effects penetrate deep into the bulk. On the other hand, if η_W is small ($l_e \gg l_i$), effects of the intrinsic anchoring prevail, causing $\phi_s \rightarrow 0°$, which again yields a very small deformation amplitude $\Delta\phi$. In between these two limits $\Delta\phi$ exhibits a maximum whose actual position depends on ε and ϕ_s (or ϕ_0).

Let us compare our dependences $\Delta\phi$ vs ϕ_s (Fig. 8) with those predicted by the phenomenological second-order elastic theory [13]. This theory predicts the proportionality $\Delta\phi \propto \sin 2\phi_s$, the characteristic length of the surface mode of the order of ρ_0, and the surface derivative $|(n_{i,j})_s| \sim 1/\rho_0$. Good quantitative agreement of our results with the theoretical prediction for the proportionality $\Delta\phi \propto \sin 2\phi_s$ takes place for small $\varepsilon\leqslant 0.01$. For $0.01\leqslant\varepsilon\leqslant 0.1$ the extremum of the calculated dependence shifts from $\phi_s=45°$ (expected for $\Delta\phi \propto \sin 2\phi_s$) to a larger value, therefore only qualitative agreement is present. However, for even larger ε also this agreement vanishes as the calculated dependence changes sign in the range $0°<\phi_s<90°$.

Let us now further explore the agreement for $\varepsilon<0.1$, where $\Delta\phi \propto \sin 2\phi_s$ is still a sufficiently good approximation, by plotting the dependence $\Delta\phi$ vs ε. If we choose $\phi_s \approx 45°$, within the second-order theory the relation $\Delta\phi \sim -k_{13}/2K$ holds [7]. The microscopic expressions for the bare splay-bend K_{13} and the Frank elastic constants are in our case found to be $K_{13}=-(J/5)\varepsilon[-1+(9/7)\varepsilon]$ and $K=(J/3)[1-(12/5)\varepsilon+(54/35)\varepsilon^2]$, where J is connected with the intermolecular interaction (for details see [35]). The ratio $-K_{13}/2K$ and, consequently, $\Delta\phi$ are therefore ε dependent too. This theoretical prediction is compared to our calculations in Fig. 9, which shows the dependence $\Delta\phi$ vs ε for nematic samples with contact and noncontact external anchoring, but only for $\varepsilon<0.1$, where the $\sin 2\phi_s$ dependence can be reproduced by our model. As it is evident from Fig. 9, the agreement is only in the functional form, but not in the deformation amplitude, if the bare K_{13} splay-bend elastic constant is used for k_{13}. In addition to the neglect of higher-order terms in the second-order theory, this can be attributed also to a possible renormalization of the bare K_{13} constant due to reduced symmetry of the nematic phase near the boundary [7] and due to surface fields [8]. The latter possibility is in agreement with a significant difference in slope of the plotted curve for contact and noncontact external anchoring.

The characteristic length of deformations found in our simulation is a few ($\sim$2–3) molecular dimensions as predicted by the second-order elastic theory. However, for our range of allowed interaction anisotropy $\varepsilon\leqslant 0.3$, the amplitude of the deformation $\Delta\phi$ is rather small. Thus the deformation is weak, although its characteristic length is still about ρ_0. The deformation strength expressed in terms of the surface director derivative $|(n_{i,j})_s|$ is, for the calculated profiles ($\varepsilon\leqslant 0.3$ and $\eta_W\lesssim 1$), always $|(n_{i,j})_s| \lesssim 2\times 10^{-2}/\rho_0 \ll 1/\rho_0$. It should be stressed that the deformations are not strong, although in the above range of parameters ε and η_W both external and intrinsic anchoring are much stronger than experimentally observed. In particular, the deformation strength is much smaller than $1/l_i$ and $1/l_e$, which are the only natural dimensional estimates. This should be attributed to the suppressing effect of higher-order elastic terms.

IV. CONCLUSION

We have studied the existence of strong subsurface deformations in nematic liquid crystals predicted by some phenomenological approaches [10] and denied by the others [9]. For this purpose we have developed a simple microscopic lattice model whose main advantages are its simplicity and the absence of the lattice-induced bulk easy axis. We started by analyzing the incomplete intermolecular interaction due to the presence of a bounding surface. This interaction gives rise to an intrinsic anchoring, which introduces a surface

easy axis. The direction of this easy axis and the anchoring strength depend on the parameter ε of the interaction anisotropy, but in the ε range in which the model is expected to work well ($\varepsilon \lesssim 0.3$), the easy axis is expected to be all the time homeotropic. The same result has been obtained also for different kinds of interaction energy: in Ref. [23], using the Gay-Berne potential, and in Ref. [22], studying the Maier-Saupe interaction between ellipsoidal molecules. The qualitative behavior of the easy axis is similar also to the preliminary results achieved with the continuous model [36], where both the interaction anisotropy and the anisotropy in shape can be varied. The estimate of the intrinsic contribution to the de Gennes–Kléman extrapolation length is for $\varepsilon \sim 0.3$ of the order of the molecular dimension ρ_0, whereas it should be, according to experimental data, at least 100 times larger. Our estimates for the extrapolation length approach the standard experimental finding in their order of magnitude only for very small values $\varepsilon \lesssim 0.01$.

Imposing an external magnetic field or external anchoring (nematic-substrate interaction) results in a deformation of the director profile. The form of the deformation can be qualitatively explained alone by the competition of the intrinsic anchoring with external forces present in the system: the magnetic field, in the former case, and external anchoring, in the latter case. For experimentally achievable magnetic fields ($\zeta \sim 100$ nm), the deformations are weak: They are relatively weak even in the case of very strong external and intrinsic anchoring, which indicates a considerable contribution of higher-order elasticity.

A subsurface deformation is produced as soon as the two competing effects exhibit different behavior (i.e., the corresponding forces are not collinear and have a different range) when penetrating from the surface into the bulk; which has been found just recently also by Teixeira [42] using the density functional approach. The dependence deformation amplitude $\Delta\phi$ versus surface tilt angle ϕ_s following from the theory of strong [13] K_{13}-term-induced subsurface deformations can be quantitatively reproduced only for small ε, where the deformations are very weak. In addition, the effective splay-bend elastic constant k_{13} seems to be considerably smaller than the bare K_{13} constant. Our analysis shows that in order to compare the extrapolation length obtained in the framework of our model and the one experimentally measured, we have to assume a small anisotropy of the interparticle interaction ($\varepsilon \lesssim 0.01$) and a rather weak surface coupling ($\eta_W \lesssim 0.01$). This also suggests $k_{13} \ll K$. In this limit the subsurface deformation still exists and is delocalized over a few molecular lengths. Consequently, the normal surface derivative of the orientation angle is small, as required by the elastic theory. This conclusion holds only if spatial variations of scalar order parameters, elastic constants, density, and impurities concentration do not considerably change the elastic properties of the nematic liquid crystal and thus prevent us from assuming that the experiment is giving the actual anchoring strength. Moreover, in our analysis we assumed temperature to be equal to zero and consequently assumed the presence of perfect nematic order. In contrast, in a real case with $T > 0$ the nematic order is no longer perfect, which is expected to effectively decrease the anisotropy of the interaction and the corresponding intrinsic anchoring strength.

Further, it should be realized that in our model we consider only the anisotropy of the van der Waals–type intermolecular interaction. However, real nematic molecules are anisotropic in shape, which gives rise to an anisotropy induced by short-range forces due to steric repulsion [37]. The latter kind of anisotropy is expected to decrease the intrinsic anchoring strength and, consequently, the deformation strength. Another complication of the interfacial behavior, which for certain intermolecular and surface interactions can occur, is surface-induced smectic ordering. This ordering has been observed in several nematic materials [38,39] and also in some model systems, even if the lattice approximation was not used [40,41]. Therefore, one must take our findings as a first step towards an understanding of the microscopic picture of subsurface deformations in the nematic liquid crystal.

ACKNOWLEDGMENTS

We wish to acknowledge the financial support from the Ministry of Science and Technology of Slovenia (Grant No. J1-7067) and from the European Union (Grants No. CIPA CT93-0159 and PECO ERBCIPDCT94-0602).

[1] F. C. Frank, Discuss. Faraday Soc. **25**, 19 (1958).
[2] C. W. Oseen, Trans. Faraday Soc. **29**, 883 (1933).
[3] H. Zocher, Trans. Faraday Soc. **29**, 945 (1933).
[4] J. Nehring and A. Saupe, J. Chem. Phys. **54**, 337 (1971).
[5] S. Faetti and M. Riccardi, Nuovo Cimento D **17**, 1019 (1995).
[6] S. Faetti and M. Riccardi, J. Phys. (France) II **5**, 1165 (1995).
[7] R. Barberi, G. Barbero, M. Giocondo, and R. Moldovan, Phys. Rev. E **50**, 2093 (1994).
[8] A. L. Alexe-Ionescu, S. Fontanini, A. M. Figueiredo-Neto, and G. Barbero, Phys. Rev. E **53**, R4299 (1996).
[9] V. M. Pergamenshchik, Phys. Rev. E **48**, 1254 (1993).
[10] C. Oldano and G. Barbero, Phys. Lett. **110A**, 213 (1985).
[11] S. Ponti, Phys. Lett. A **200**, 165 (1995).
[12] S. Stallinga and G. Vertogen, Phys. Rev. E **53**, 1692 (1996).
[13] G. Barbero, A. Sparavigna, and A. Strigazzi, Nuovo Cimento D **12**, 1259 (1990).
[14] S. Faetti, Phys. Rev. E **49**, 4192 (1994;); **49**, 5332 (1994).
[15] I. Dahl and A. de Meyere, Liq. Cryst. **18**, 683 (1995).
[16] H. P. Hinov, Mol. Cryst. Liq. Cryst. **148**, 197 (1987).
[17] V. M. Pergamenshchik, P. I. C. Teixeira, and T. J. Sluckin, Phys. Rev. E **48**, 1265 (1993).
[18] G. Barbero, L. R. Evangelista, and S. Ponti, Phys. Rev. E **53**, 1256 (1996).
[19] P. Galatola, C. Oldano, M. Rajteri, and G. Barbero, Phys. Lett. A **210**, 101 (1996).
[20] M. Rajteri, G. Barbero, P. Galatola, C. Oldano, and S. Faetti, Phys. Rev. E **53**, 6093 (1996).
[21] W. Maier and A. Saupe, Z. Naturforsch. A **14**, 882 (1959); **15**, 287 (1960).

[22] L. R. Evangelista and S. Ponti, Phys. Lett. A **197**, 55 (1995).
[23] J. Stelzer, L. Longa, and H. R. Trebin, J. Chem. Phys. **103**, 3098 (1995).
[24] P. A. Lebwohl and G. Lasher, Phys. Rev. A **6**, 426 (1972).
[25] L. F. Rull, Physica A **220**, 113 (1995).
[26] A. Rapini and M. Papoular, J. Phys. (Paris) Colloq. **30**, C4-54 (1969).
[27] P. G. de Gennes and J. Proust, *The Physics of Liquid Crystals* (Clarendon, Oxford 1993).
[28] S. Faetti and M. Nobili, J. Phys. (France) II **4**, 1617 (1994).
[29] L. M. Blinov, A. Yu. Kabayenkov, and A. Sonin, Liq. Cryst. **5**, 263 (1989).
[30] S. Ponti and L. R. Evangelista, Liq. Cryst. **20**, 105 (1996).
[31] A. L. Alexe-Ionescu, G. Barbero, and A. G. Petrov, Phys. Rev. E **48**, R1631 (1993).
[32] H. Yokoyama, S. Kobayashi, and H. Kamei, J. Appl. Phys. **61**, 4501 (1987).
[33] G. Barbero and G. Durand, J. Appl. Phys. **69**, 6968 (1991).
[34] B. Jérôme, Rep. Prog. Phys. **54**, 391 (1991).
[35] G. Barbero, Mol. Cryst. Liq. Cryst. **195**, 199 (1991).
[36] G. Skačej, A. L. Alexe-Ionescu, and S. Žumer (unpublished).
[37] J. C. Gay and B. J. Berne, J. Chem. Phys. **74**, 3316 (1981).
[38] C. Rosenblatt, Phys. Rev. Lett. **53**, 791 (1984).
[39] B. M. Ocko, Phys. Rev. Lett. **64**, 2160 (1990).
[40] Z. Zhang, A. Chakrabarti, O. G. Mouritsen, and M. J. Zuckermann, Phys. Rev. E **53**, 2461 (1996).
[41] J. Stelzer, P. Galatola, G. Barbero, and L. Longa (unpublished).
[42] P. I. C. Teixeira, Phys. Rev. E **55**, 2876 (1997).